

This is the accepted manuscript made available via CHORUS. The article has been published as:

Electronic doping of graphene by deposited transition metal atoms

Jaime E. Santos, Nuno M. R. Peres, João M. B. Lopes dos Santos, and António H. Castro Neto

Phys. Rev. B **84**, 085430 — Published 26 August 2011

DOI: [10.1103/PhysRevB.84.085430](https://doi.org/10.1103/PhysRevB.84.085430)

Electronic doping of graphene by deposited transition metal atoms

Jaime E. Santos^{1,3}, Nuno M. R. Peres², João M. B. Lopes dos Santos³ and António H. Castro Neto^{4,5}

¹ *Max Planck Institute for the Physics of Complex Systems, Nöthnitzer Str. 38, D-01187 Dresden, Germany;* ² *Centro de Física and Departamento de Física, Universidade do Minho, P-4710-057 Braga, Portugal;* ³ *CFP and Departamento de Física, Faculdade de Ciências, Universidade do Porto, 4169-007 Porto, Portugal;* ⁴ *Department of Physics, Boston University, 590 Commonwealth Avenue, Boston, Massachusetts 02215, USA;* ⁵ *Graphene Research Centre, and Department of Physics, National University of Singapore, 2 Science Drive 3, 117542, Singapore; **
(Dated: today)

We perform a phenomenological analysis of the problem of the electronic doping of a graphene sheet by deposited transition metal atoms, which aggregate in clusters. The sample is placed in a capacitor device such that the electronic doping of graphene can be varied by the application of a gate voltage and such that transport measurements can be performed via the application of a (much smaller) voltage along the graphene sample, as reported in the work of²⁶. The analysis allows us to explain the thermodynamic properties of the device, such as the level of doping of graphene and the ionisation potential of the metal clusters in terms of the chemical interaction between graphene and the clusters. We are also able, by modelling the metallic clusters as perfect conducting spheres, to determine the scattering potential due to these clusters on the electronic carriers of graphene and hence the contribution of these clusters to the resistivity of the sample. The model presented is able to explain the measurements performed by²⁶ on Pt-covered graphene samples at the lowest metallic coverages measured and we also present a theoretical argument based on the above model that explains why significant deviations from such a theory are observed at higher levels of coverage.

PACS numbers: 73.22.Pr, 72.80.Vp, 73.30.+y

Keywords: Transport in graphene, Transition Metals, Metallic Clusters

I. INTRODUCTION

Graphene was discovered in late 2004^{1,2}. This material is a one-atom thick sheet of carbon atoms, arranged in a honeycomb lattice. This structure is not a Bravais lattice and graphene is described in terms of a triangular lattice with a two-atom basis. A simple nearest-neighbour tight-binding approximation of the electronic Hamiltonian in graphene reveals that such lattice structure leads to a dispersion relation that is linear around two specific points of the Brillouin zone. Since the Fermi level of graphene lies at these points, its quasi-particles behave in a continuum approximation as massless relativistic fermions with a speed of light equal to the Fermi-velocity $\approx 10^6 \text{ms}^{-1}$ (see³ and the recent review⁴).

The properties of graphene and its special geometry make it a very interesting candidate for applications in nano-electronics. Recent research has revealed other possible applications, in solar cell technology⁵, in liquid crystal devices⁶, in single molecule sensors⁷, and in the fabrication of nano-sized prototype transistors⁸.

Transport measurements on graphene devices¹ have become standard and can be performed under different doping conditions. Given the location of the Fermi level and the absence of a band gap between the valence and conduction bands in undoped graphene, one can continuously control the level of doping simply by the application of a gate voltage in a geometry where graphene acts as the upper (grounded) electrode of a capacitor. The lower electrode is composed of silicon, whereas the dielectric medium in between is SiO_2 . Metal contacts placed on top of the graphene sheet allow for the realisation of transport measurements at different gate voltages, and hence at different levels of doping, with great flexibility. The system has an overall thickness of $b \approx 300 \text{ nm}$ (see figure 1).

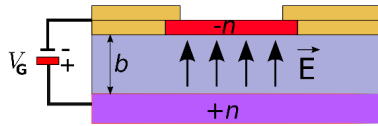


FIG. 1: Capacitor device whose upper electrode is a single graphene sheet. The application of a gate voltage imposes a certain level of electron or hole doping on graphene, continuously increasing or lowering its Fermi level. The application of a potential difference between the upper contacts allows for transport measurements to be performed.

The measurement of the transport properties using such devices can be used to determine the influence of different physical effects on both the AC and DC conductivities. One can investigate the influence of electron-electron interactions, of impurities, or of the presence of elastic ripples in the graphene sheet on the transport properties of this semi-metal³.

It is well known that undoped graphene, when analysed from the point of view of a self-consistent theory or the renormalisation group, presents a finite conductivity with an universal value of $4e^2/(\pi h)^{9-18}$, regardless of the scattering mechanism that limits conductivity in graphene. The experimental measurements^{19,20} point to a somewhat higher value for this quantity, equal to $4e^2/h$. This latter value is also obtained in studies of numerical diagonalisation of graphene's tight-binding Hamiltonian with add-atoms acting as the source of disorder^{21,22}. In the case of doped graphene, the behaviour of the conductivity markedly depends on the scattering mechanism that limits such quantity. It is therefore essential to clarify the nature of such a mechanism. The research community has held two opposing views, namely charged (Coulomb) or short-range scatterers²³, but recent experiments²⁴ seem to show the latter mechanism as the prevailing one, even if it is agreed that charged scatterers also play a role²⁵.

In this paper, we will consider the contribution to the conductivity of one particular type of short-range disorder, namely that induced by the deposition of transition metal (TM) atoms in graphene²⁶. This type of disorder is always present on devices such as those depicted in figure 1, due to the diffusion of metallic atoms from the contacts into the graphene sheet. The adsorption of graphene on TM surfaces has been extensively studied, both experimentally²⁷⁻³⁰, as well as theoretically³¹⁻³⁶. In TM surfaces for which the adsorption process (physisorption) preserves the conical nature of the graphene bands close to the Dirac point (Al, Ag, Cu, Au, Pt), the authors of^{35,36} have shown that the levels of electron or hole doping of graphene that they have found in their DFT studies can be explained by the relative value of the bulk work-functions of graphene and of that of the transition metal to which graphene is adsorbed. However, in order to explain the electron-doping of graphene in cases where its work-function is lower than that of the transition metal (Ag, Cu), the authors invoked the existence of a chemical interaction between graphene and the underlying metal substrate, which plays a significant role in the formation of surface dipoles³⁷⁻⁴². The existence of such an interaction was confirmed in the experimental transport studies of²⁶, performed on a graphene sheet where TM atoms were deposited, which was part of device such as that of figure 1. The authors of this study have found that in the case of low coverage of graphene by Pt, the metal with the highest work function studied theoretically by^{35,36}, graphene is also electronically doped by Pt, becoming hole-doped at higher coverages. The authors stated that the high levels of electron-doping that they have found at low coverages were caused by an increased chemical interaction between graphene and the TM atoms, due to the short-distance (less than 3 Å) between the two species (this distance is equal to 3.3 Å in the full coverage regime). Furthermore, the AFM pictures obtained seem to show that the transition metal atoms aggregate in clusters at low coverage (see also⁴³). It is nevertheless unclear whether the proximity between the clusters and graphene is sufficient to justify the level of doping of graphene.

The purpose of this paper is threefold. Firstly, we wish to introduce a framework that allow us to discuss the problem of charge doping of graphene by transition-metal clusters with generality from a thermodynamic point of view. This framework will be of a phenomenological nature and it will involve some simplifying assumptions, but it will already contain the main ingredients that will need to be considered in a more fundamental approach. Secondly, the same type of phenomenological analysis will be extended to the problem of electronic scattering in graphene caused by the presence of the said clusters. We will show, following⁴⁴ that, despite the charged nature of the clusters, the scattering potential that they create is of a short-ranged nature (see also²³). The domain of validity of the semi-classical approximation of independent clusters that we are using is also discussed. Thirdly, these two elements of the theory will be used to interpret the above experiments from a quantitative point of view. This application of the theory will also serve to illustrate its overall limitations and we will provide physical arguments that show why more elaborate approaches are needed.

The structure of this paper is as follows: in section II, we will discuss the doping of graphene by metal clusters in a capacitor device based on a phenomenological model that treats each cluster as a perfectly metallic object kept at a constant potential dependent on the amount of charge in the cluster. The minimisation of the internal energy of the system at $T = 0$, subjected to overall charge conservation, will allow us to obtain the equilibrium conditions that determine the level of doping of the graphene sheet. One can show, for equally charged clusters, that the level of doping can be written in terms of the bulk work-functions of the different components of the system, of the gate voltage applied to the device, and of a parameter that characterises the *effective* chemical interaction between the graphene sheet and each individual cluster. The numerical value of this parameter is determined by two different contributions: the first contribution is due to the induced surface dipole of graphene and of the metallic clusters caused by the presence of the other components of the system; the second contribution is the correction to the Fermi energy of a cluster due to its finite size. Specialising to the case of spherical clusters, we can estimate the magnitude of the chemical interaction using the measured values by²⁶ of the gate voltage that is necessary to apply to Pt and Ti-covered⁴⁵ graphene samples to bring graphene to an uncharged state, where the conductivity is a minimum. These values are dependent on the concentration of metallic atoms per unit cell as well as on which metallic element is deposited on graphene. In section

III, we will consider the form of the scattering potential created by a spherical cluster, following the model of⁴⁴ and its contribution to the resistivity of the sample, within the First Born Approximation (FBA) and we will compare our results with the transport measurements of²⁶, performed on Pt-covered graphene samples at low coverage. We will also show why the theory presented is not adequate to explain the measurements performed at higher coverages, both for Pt and Ti-covered samples. We will determine, using the above model, the linear dimension of the region in graphene where the charge donated by the cluster to this material is contained and show that, except for the lowest coverages considered in the experiments of²⁶, this quantity is comparable to the average distance between clusters, even for heavily-doped graphene. In section IV, we will present our conclusions. In appendix A, we will derive an expression for the cluster's ionisation potential that will be used in the main text, based on the same thermodynamic arguments that were used in section II. Finally, in appendix B, we will derive, using the method of images, the electrostatic contribution to the ionisation potential of a single spherical cluster, a result that will be shown to be in agreement with that of appendix A. This derivation will also allow us to obtain the capacitance of the system composed of the metallic cluster and of the graphene plane, as well as the electrostatic potential due to a charged spherical cluster close to a grounded plane, a quantity that enters in the calculations performed in section III.

II. ELECTRONIC DOPING OF GRAPHENE BY DEPOSITED METAL CLUSTERS

At $T = 0$, the internal energy of a composite system of k conductors can be written^{46,47}, assuming that the electrons and the (immobile) ions of the different species interact with each other via the bare Coulomb interaction (i.e. one is including the contribution of the low lying electronic orbitals explicitly in the energy), as

$$\mathcal{E} = G(N_1, \dots, N_k) + \frac{1}{2} \sum_{i,j} \int_{V_i} d^d r \int_{V_j} d^d r' \frac{\rho_i^P(\mathbf{r}) \rho_j^P(\mathbf{r}')}{4\pi\epsilon_0 |\mathbf{r} - \mathbf{r}'|}, \quad (1)$$

where the functional $G(N_1, \dots, N_k)$ includes the kinetic, exchange and correlation energies of the electrons and where the second term includes the effect of the ion potential on the electrons and the Hartree energy of these electrons, with $\rho_i^P(\mathbf{r}) = \rho_i^e(\mathbf{r}) - \rho_i^{ions}(\mathbf{r})$ being the plasma charge density. The indices i, j run over $1, \dots, k$. One can write $\rho_i^P(\mathbf{r}) = \rho_i^n(\mathbf{r}) + \delta\rho_i(\mathbf{r})$, where $\rho_i^n(\mathbf{r})$ is the charge density in the neutral ground state of each conductor and $\delta\rho_i(\mathbf{r})$ is the excess charge density of that conductor due to charge exchange with the others. In particular, $\int_{V_i} d^d r \delta\rho_i(\mathbf{r}) = Q_i$, the total unbalanced charged contained in conductor i . Using this decomposition, one can write the ground-state energy, up to a constant term, as

$$\mathcal{E} = G(N_1, \dots, N_k) + \sum_i \int_{V_i} d^d r \mathcal{V}_i^n(\mathbf{r}) \delta\rho_i(\mathbf{r}) + \frac{1}{2} \sum_{i,j} \int_{V_i} d^d r \int_{V_j} d^d r' \frac{\delta\rho_i(\mathbf{r}) \delta\rho_j(\mathbf{r}')}{4\pi\epsilon_0 |\mathbf{r} - \mathbf{r}'|}, \quad (2)$$

where $\mathcal{V}_i^n(\mathbf{r})$ is the potential on conductor i due to itself and the other conductors, each in a neutral state. In a classical approximation, $\delta\rho_i(\mathbf{r})$ will be non-zero only close to the surface of the conductors, and we can write the above expression in a capacitor approximation:

$$\mathcal{E} = G(N_1, \dots, N_k) + \sum_i D_i Q_i + \frac{1}{2} \sum_{i,j} C_{ij}^{-1} Q_i Q_j, \quad (3)$$

where C_{ij}^{-1} is the inverse cross-capacitance between conductors i and j and $D_i = \overline{\mathcal{V}_i^n(\mathbf{r})}$ is the surface dipole of conductor i ⁴¹, which is the average value of the electrostatic potential within that conductor. Note that the surface dipole of a conductor is computed with the remaining conductors present, but in a neutral state. Thus, one expects that such surface dipoles will depend both on the geometry of each conductor and also on the presence of the other conductors if the distances between them are on the atomic scale.

As stated above, the experiments of reference²⁶ were performed on a devices similar to that depicted in figure 1, with the transition metal atoms deposited by molecular beam epitaxy (MBE) on the graphene sheet at different coverages $c_S = N_{am}/n_u$ of metallic atoms per unit cell of graphene, where N_{am} is the total number of deposited

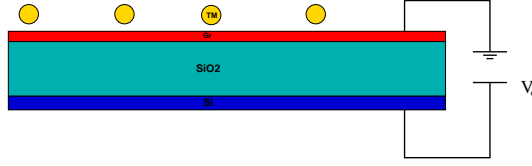


FIG. 2: Schematic representation of model that is considered in this paper. Transport measurements can be performed at different coverages as more atoms are deposited by MBE.

metallic atoms and n_u is the number of graphene's unit cells. In order to model such a device, we will assume that the atoms aggregate in N_c identical clusters, which are randomly distributed above the area $A_g = n_u A_c$ of the graphene sheet, where A_c is the area of the graphene unit cell. We also assume that these clusters are all equally charged. The graphene sheet is kept at zero potential. At a distance $b \approx 300$ nm below it, one places a Si layer, with the space in between filled with SiO_2 , a medium of permittivity $\epsilon = 3.9 \epsilon_0$. The graphene sheet and the Si layer are connected to a battery such that a constant gate-voltage V_G is kept between them ('plane-capacitor model', see figure 2). A single cluster-graphene subsystem is assumed to possess a joint capacitance C_S (which is computed for spherical clusters in appendix B). The capacitance of the graphene/ SiO_2 /Si device is given by $C_{Si} = \epsilon A_g / b$. We assume that the cross-capacitance effects between different clusters are only due to the presence of the grounded graphene plane, an assumption that is correct for small C_S ⁴⁸. With such assumptions, the internal energy (3) can be written for this system, as

$$\begin{aligned} \mathcal{E} = & G(N_S, \dots, N_S, N_g, N_{Si}) - e N_c D_S (N_S - N_S^0) \\ & - e D_g (N_g - N_g^0) - e D_{Si} (N_{Si} - N_{Si}^0) \\ & + \frac{e^2 N_c}{2C_S} (N_S - N_S^0)^2 + \frac{e^2}{2C_{Si}} (N_{Si} - N_{Si}^0)^2. \end{aligned} \quad (4)$$

We have written the charge Q_i of a given component i as $Q_i = -e(N_i - N_i^0)$, where N_S , N_g and N_{Si} are, respectively, the number of electrons in a cluster (all clusters are equally charged), in graphene and in the Si layer in the equilibrium state in which these materials are in contact and exchange charge, and N_S^0 , N_g^0 and N_{Si}^0 are the same quantities in the uncharged state of these materials. Also, D_S , D_g and D_{Si} are the surface dipoles of each substance.

The conditions of thermodynamic equilibrium are obtained through the minimisation of (4) subjected to the constraints that the overall charge of the system is zero and that the potential difference between the two electrodes of the battery is equal to V_G . The minimisation condition is thus given by

$$d\mathcal{E} = -eV_G dN_{Si} + \mu (N_c dN_S + dN_g + dN_{Si}), \quad (5)$$

since the charge transferred between the electrodes of the battery is $dq = -e dN_{Si}$, and where μ is the chemical potential of the system. One obtains from (5) the following equilibrium conditions

$$\bar{\mu}_g = \bar{\mu}_S + e(D_g - D_S) + \frac{e^2(N_S - N_S^0)}{C_S}, \quad (6)$$

$$\bar{\mu}_g = \bar{\mu}_{Si} + e(D_g - D_{Si}) + eV_G + \frac{e^2(N_{Si} - N_{Si}^0)}{C_{Si}}, \quad (7)$$

where $\bar{\mu}_S = \frac{\partial G}{\partial N_j} |_{N_j=N_S}$, with N_j being the number of charges in cluster j , $\bar{\mu}_g = \frac{\partial G}{\partial N_g}$, $\bar{\mu}_{Si} = \frac{\partial G}{\partial N_{Si}}$, are the chemical potentials of the different components of the system in the absence of a dipole layer. These quantities are also called the internal contribution of a metal to its work-function³⁷. Note that $\mu = \bar{\mu}_g - eD_g$, i.e. the chemical potential of the system is equal to the (full) chemical potential of the subsystem kept at zero voltage.

The two equilibrium conditions (6,7) are not sufficient to determine the level of doping of the constituents of the system. These equations have to be supplemented with the neutrality condition for the overall system. One can write this condition as

$$N_c \Delta N_S + \Delta N_g + \Delta N_{Si} = 0, \quad (8)$$

with $\Delta N_S = N_S - N_S^0$, $\Delta N_g = N_g - N_g^0$ and $\Delta N_{Si} = N_{Si} - N_{Si}^0$. The quantities that appear in (8) are related to the variations of the carrier density of the cluster, of graphene, and of the Si layer, by $\Delta N_S = \mathcal{V}_S \delta n_S$, $\Delta N_g = A_g \delta n_g$

and $\Delta N_{Si} = A_g \delta n_{Si}$, where \mathcal{V}_S is the volume of the cluster. The number of clusters is given by $N_c = N_{am}/n_{amc}$, where n_{amc} is the number of metal atoms per cluster, which is equal to $n_{amc} = z_S \mathcal{V}_S / v_S$, with v_S being the volume of the metallic unit cell and z_S being the number of atoms in the unit cell ($z_S = 1$ for Pt, $z_S = 2$ for Ti). Expressing N_{am} in terms of c_S , which was introduced at the beginning of this section, one obtains for N_c

$$N_c = \frac{c_S v_S A_g}{z_S \mathcal{V}_S A_c}, \quad (9)$$

where we have expressed n_u as the ratio between the area of the graphene sheet and the unit cell area. Substituting this formula in equation (8) and expressing ΔN_S , ΔN_g and ΔN_{Si} in terms of the variations of the charge density of each media, one obtains

$$\frac{c_S v_S}{z_S A_c} \delta n_S + \delta n_g + \delta n_{Si} = 0. \quad (10)$$

The equations (6,7), when written in terms of the variations of density δn_S and δn_{Si} , become

$$\bar{\mu}_g = \bar{\mu}_S + e(D_g - D_S) + \frac{e^2 \mathcal{V}_S}{C_S} \delta n_S, \quad (11)$$

$$\bar{\mu}_g = \bar{\mu}_{Si} + e(D_g - D_{Si}) + eV_G + \frac{e^2 b}{\epsilon} \delta n_{Si}, \quad (12)$$

These two equations, which impose the equality of the so-called electro-chemical potentials⁴⁹ between a metallic cluster and the graphene sheet, and between the graphene sheet and the Si layer, when supplemented by (10), are sufficient to determine the level of doping of graphene. However, we still need to relate the chemical potential $\bar{\mu}_S$ to δn_S , $\bar{\mu}_g$ to δn_g and $\bar{\mu}_{Si}$ to δn_{Si} , in other words, we need the equation of state for the different components of the system. One writes $\Delta \varepsilon_F^S = \bar{\mu}_S - \varepsilon_F^S$ for the Fermi energy variation of the cluster, $\Delta \varepsilon_F^g = \bar{\mu}_g - \varepsilon_F^g$ for the Fermi energy variation of graphene and $\Delta \varepsilon_F^{Si} = \bar{\mu}_{Si} - \varepsilon_F^{Si}$ for the Fermi energy variation of the Si layer, measured with respect to the uncharged ground state of each of these constituents. In the case of the clusters or of the Si layer, one has $\delta n_S \approx \rho_S(\varepsilon_F^S) \Delta \varepsilon_F^S$ and $\delta n_{Si} \approx \rho_{Si}(\varepsilon_F^{Si}) \Delta \varepsilon_F^{Si}$ since the density of states $\rho(\varepsilon_F)$ is approximately constant for these materials at the Fermi level. Substituting these definitions in (11) and (12) and taking into account that the bulk work functions of the transition metal, of graphene, and of Si, are given by $W_B = eD_B - \varepsilon_F^B$, $W_g^0 = eD_g^0 - \varepsilon_F^g$ and $W_{Si}^0 = eD_{Si}^0 - \varepsilon_F^{Si39}$, one obtains

$$\delta n_S = \frac{W_B - W_g^0 - e(\Delta D_g - \Delta D_S) - \zeta_S + \Delta \varepsilon_F^g}{1/\rho_S(\varepsilon_F^S) + e^2 \mathcal{V}_S / C_S}, \quad (13)$$

$$\delta n_{Si} = \frac{W_{Si}^0 - W_g^0 + e(\Delta D_{Si} - \Delta D_g - V_G) + \Delta \varepsilon_F^g}{1/\rho_{Si}(\varepsilon_F^{Si}) + e^2 b / \epsilon}, \quad (14)$$

where $\zeta_S = \varepsilon_F^S - \varepsilon_F^B$ is the difference between the Fermi energy of the TM cluster and the Fermi energy of the bulk transition-metal and $\Delta D_S = D_S - D_B$, $\Delta D_g = D_g - D_g^0$ and $\Delta D_{Si} = D_{Si} - D_{Si}^0$ are the induced surface dipoles on each component of the system due to finite size effects and to the presence of the other components. One can estimate $\rho_{Si}(\varepsilon_F^{Si}) \approx \frac{m_{Si}^*}{\pi \hbar^2}$, the result for a free two-dimensional electron gas, where $m_{Si}^* \approx m_e$ is the electron's effective mass in Si. With $b \approx 300$ nm, one has $\rho_{Si}(\varepsilon_F^{Si}) \gg \epsilon / (e^2 b)$ and one can neglect the first term in the denominator of (14). One can thus write (13,14) as

$$\delta n_S = \frac{W_B - W_g^0 - \Delta_c + \Delta \varepsilon_F^g}{1/\rho_S(\varepsilon_F^S) + e^2 \mathcal{V}_S / C_S}, \quad (15)$$

$$\delta n_{Si} = \frac{\epsilon}{e^2 b} [e(V_0 - V_G) + \Delta \varepsilon_F^g], \quad (16)$$

where $\Delta_c = \zeta_S + e(\Delta D_g - \Delta D_S)$ represents a correction to the doping of the clusters due to their finite size and to the induced surface dipoles, and $V_0 = (W_{Si}^0 - W_g^0)/e + \Delta D_{Si} - \Delta D_g$. The quantity Δ_c can be interpreted as giving the overall magnitude of the *effective* chemical interaction between the clusters and the graphene sheet.

The density of states $\rho_g(\epsilon)$ of graphene is zero at the Dirac point and one needs to consider its full functional form in that neighbourhood. It is approximately given by²⁵

$$\rho_g(\epsilon) = \frac{4}{\sqrt{3} \pi t^2 A_c} |\epsilon - \varepsilon_F^g|, \quad (17)$$

where $t = 2.7$ eV is the first-nearest neighbour hopping matrix element in graphene. Note that the presence of impurities in graphene, either intrinsic or the deposited TM atoms themselves, will modify the density of states given in (17) for high enough impurity concentrations¹⁶. Integrating $\rho_g(\varepsilon)$ between the lower band limit $\varepsilon_F^g - \sqrt{\sqrt{3}\pi t}$ and the Fermi energy ε_F^g ¹⁵ yields a result of two electrons per unitary cell.

Integrating $\rho_g(\varepsilon)$ between ε_F^g and μ_g , one obtains for δn_g the result

$$\delta n_g = \pm \frac{2}{\sqrt{3}\pi t^2 A_c} (\Delta \varepsilon_F^g)^2. \quad (18)$$

with the plus sign if $\Delta \varepsilon_F^g > 0$ and the minus sign otherwise.

Substituting equations (15), (16) and (18) in (10), we finally obtain a second-degree equation for $\Delta \varepsilon_F^g$

$$\pm (\Delta \varepsilon_F^g)^2 + \Lambda \Delta \varepsilon_F^g - \Omega = 0, \quad (19)$$

with the plus sign if $\Delta \varepsilon_F^g > 0$ and negative sign otherwise, and where

$$\Lambda = \frac{\sqrt{3}\pi t^2}{2} \left[\frac{c_S v_S}{z_S(1/\rho_S(\varepsilon_F^S) + e^2 \mathcal{V}_S/C_S)} + \frac{\epsilon A_c}{e^2 b} \right], \quad (20)$$

$$\Omega = \frac{\sqrt{3}\pi t^2}{2} \left[\frac{c_S v_S (W_g^0 + \Delta_c - W_B)}{z_S(1/\rho_S(\varepsilon_F^S) + e^2 \mathcal{V}_S/C_S)} + \frac{\epsilon A_c}{e b} (V_G - V_0) \right]. \quad (21)$$

If we take the positive sign in equation (19) then a positive solution exists if $\Omega > 0$. Conversely, if we take the negative sign in this equation, a negative solution exists if $\Omega < 0$. One can thus write for $\Delta \varepsilon_F^g$, the solution⁵⁰

$$\Delta \varepsilon_F^g = \text{sign}(\Omega) \left(\sqrt{\frac{\Lambda^2}{4} + |\Omega|} - \frac{\Lambda}{2} \right). \quad (22)$$

One can see from equation (22) that for a given concentration c_S , one can, through the application of a gate-voltage V_D such that $\Omega = 0$, bring the graphene sheet to its uncharged state, as $\Delta \varepsilon_F^g = 0$. The gate voltage V_D can be determined from transport measurements on Pt or Ti-covered graphene²⁶, since the conductivity will display the minimum characteristic of the Dirac point for that applied voltage. Likewise, the gate voltage V_0 can be determined from the same measurements performed on the uncovered graphene samples, since it follows from equation (22) that for $c_S = 0$, $\Delta \varepsilon_F^g = 0$ at $V_G = V_0$. Thus, the conductivity will also display the characteristic minimum at this applied voltage. Therefore, one can extract Δ_c from experiment. It is given by

$$\Delta_c = W_B - W_g^0 - \frac{\epsilon z_S A_c (1/\rho_S(\varepsilon_F^S) + e^2 \mathcal{V}_S/C_S)(V_D - V_0)}{e b c_S v_S}. \quad (23)$$

The density of states at the Fermi level of bulk Pt or bulk Ti can be extracted from specific heat measurements^{51,52}, through $\rho(\varepsilon_F^B) = 3\gamma/(\pi k_B)^2$, using the general result from Landau's Fermi liquid theory, where γ is the linear coefficient for the dependence of the electronic specific heat c_V on the temperature. Finite size corrections to the bulk density of states may be estimated for a spherical cluster, using the results for a free-electron gas⁵³, as $\rho_S(\varepsilon_F^S) = \rho(\varepsilon_F^B) - 3m^*/(8\pi\hbar^2 R)$, where $m_{Pt}^* \approx 2m_e$ ⁵⁴, $m_{Ti}^* \approx 3.15m_e$ ⁵² is the electron's effective mass in platinum or titanium and R is the radius of the cluster. Also, for a spherical cluster, $\mathcal{V}_S = 4\pi R^3/3$ and C_S can be written as a power series on a parameter dependent on the cluster radius and on the distance L of its centre to the graphene sheet (see appendix B). We take $W_g^0 = 4.5$ eV as in²⁶, $W_{Pt}^0 = 5.64$ eV and $W_{Ti}^0 = 4.33$ eV for polycrystalline platinum and polycrystalline titanium, and $W_{Si}^0 = 4.6$ eV⁵⁵. We note that the model as defined contains two unknown parameters, namely R and L .

Using these results, as well as the values of c_S , V_0 and V_D measured by²⁶ (raw data is a courtesy of Kawakami's group) and taking the radius of the cluster to be 0.6 nm for Pt⁵⁶ and 0.188 nm for Ti⁵⁷ and the distance from the centre of the cluster to the plane equal to 0.85 nm for Pt and 0.44 nm for Ti, one obtains for Δ_c the results given in tables I, II and III. Note that one does not dispose of direct information (e.g. from AFM measurements) regarding the values of R and L . The values indicated above were chosen such as to provide agreement between the values of Δ_c and Δ_c^{est} in tables I, II and III, as well as between the theoretical and experimental asymptotic values for the

c_S	V_D (V)	R (nm)	Δ_c (eV)	Δ_c^{est} (eV)	p_S
0.025	-11.4	0.6	2.47	2.55	-0.014
0.071	-29.0	0.6	2.49	2.55	-0.014
0.127	-46.0	0.6	2.37	2.55	-0.013

TABLE I: Values of the concentration of Pt atoms per unit cell of graphene c_S and applied voltages V_D corresponding to the minimum of conductivity for the Pt-1 sample studied in²⁶ ($V_0 = -1.94$ V). The values of Δ_c were determined using formula (23). We have also computed the number of electrons p_S per Pt atom at the Dirac point. This number was estimated in²⁶ as -0.014 e/Pt atom.

c_S	V_D (V)	R (nm)	Δ_c (eV)	Δ_c^{est} (eV)	p_S
0.0065	1.56	0.6	2.16	2.55	-0.011
0.019	-2.56	0.6	2.26	2.55	-0.012
0.039	-11.0	0.6	2.45	2.55	-0.014
0.064	-24.3	0.6	2.66	2.55	-0.016

TABLE II: Values of the concentration of Pt atoms per unit cell of graphene c_S and applied voltages V_D corresponding to the minimum of conductivity for the Pt-3 sample studied in²⁶ ($V_0 = 3.41$ V). The values of Δ_c were determined using formula (23). We have also computed the number of electrons p_S per Pt atom at the Dirac point. This number was estimated in²⁶ as -0.019 e/Pt atom.

contribution to the resistivity coming from the presence of the clusters⁵⁸ (see section III). We have considered here and below the measurements made with samples Pt-1, Pt-3 and Ti-1 (in the notation of²⁶), since these samples, when uncovered, presented the smallest values of V_0 measured, indicating a low level of intrinsic disorder.

One can estimate the correction to the Fermi energy, due to the cluster's finite radius, from the free-electron gas result, as $\zeta_S \approx \frac{3\pi^2\hbar^4}{8(m^*)^2R} \cdot \rho(\varepsilon_F^B)$. Using the result quoted in the references^{35,36} for the induced dipole $e(\Delta D_g - \Delta D_S) \approx 0.9$ eV⁵⁹, one obtains for Δ_c^{est} the results presented in tables I, II and III for Pt and Ti, respectively. Thus, it is seen that the larger value of the chemical interaction Δ_c with respect to the case studied in^{35,36} (particularly in platinum that has a larger DOS at the Fermi level) is due to a large shift of the Fermi energy of the clusters with respect to that of the bulk TM metal, caused by their finite radius.

For a small cluster, the concept of work-function is ill-defined⁶⁰, as this quantity depends on the cluster's charge. One then speaks, respectively, of the cluster's ionisation potential if one is withdrawing an electron from a cluster at equilibrium, or of the cluster's electron affinity, if the electron is withdrawn from a negatively over-charged cluster. In appendix A, we compute the ionisation potential of a cluster based on a thermodynamic argument. We obtain from (A4) the result

$$I_S = W_g^0 + e\Delta D_g + \frac{e^2}{2C_S} - \Delta\varepsilon_F^g, \quad (24)$$

for the ionisation potential of the metallic cluster, where $\Delta\varepsilon_F^g$ is given by (22). Substituting in (24) the parameters as computed in table I, we have plotted in Figures 3, 4 and 5 the result (24) as function of the applied voltage, for the different coverages c_S considered in²⁶, for their Pt-1, Pt-3 and Ti-1 samples⁶¹. In these plots, we have ignored the (unknown) constant $e\Delta D_g$ ⁶². Nevertheless, such constant shift should be obtainable from a plot of the experimental ionisation potential, and so provide an estimate of $e\Delta D_g$.

It is also shown in appendix A that the electron affinity A_S of a metallic cluster is given by $A_S = I_S - e^2/C_S$, with $W_g = \frac{1}{2}(I_S + A_S)$. Thus, $A_S < W_g < I_S$. Since the transfer of an electron from the cluster to graphene would cost an energy $I_S - W_g > 0$ and, conversely, the transfer of an electron from graphene to the cluster would cost the same energy $W_g - A_S > 0$, one sees that the equilibrium state defined by equations (10) to (12) is indeed a stable one. The theory exposed in this section constitutes the main result of this paper.

III. SCATTERING OF ELECTRONS BY THE METALLIC CLUSTERS AND ITS CONTRIBUTION TO THE RESISTIVITY IN THE FBA

In the previous section, we have computed the level of doping of a graphene sheet due to the presence of metallic clusters. We have also computed the ionisation potential of a single cluster. These properties are equilibrium proper-

c_S	V_D (V)	R (nm)	Δ_c (eV)	Δ_c^{est} (eV)	p_S
0.0038	-18.6	0.19	1.70	1.83	-0.179
0.0077	-41.0	0.19	1.89	1.83	-0.198
0.0115	-61.0	0.19	1.89	1.83	-0.198
0.0153	-73.5	0.19	1.71	1.83	-0.180
0.0191	-82.4	0.19	1.52	1.83	-0.161

TABLE III: Values of the concentration of Ti atoms per unit cell of graphene c_S and applied voltages V_D corresponding to the minimum of conductivity for the Tt-1 sample studied in²⁶ ($V_0 = -0.57$ V). The values of Δ_c were determined using formula (23). We have also computed the number of electrons p_S per Ti atom at the Dirac point. This number was estimated in²⁶ as -0.174 e/Ti atom.

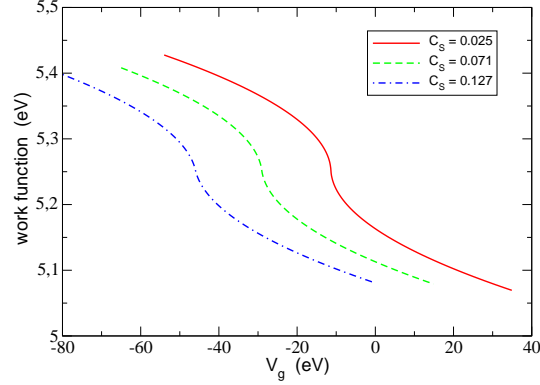


FIG. 3: Ionisation potential of cluster as a function of the applied gate voltage, for the Pt-1 sample, with coverages $c_S = 0.025, 0.071$ and 0.127 ML (rgb).

ties. However, the experiments of²⁶ measured the dependence of the conductivity of graphene on the doping induced by the metallic clusters and by the applied gate voltage. In order to describe such dependence, one needs to determine the scattering potential on individual carriers due to the presence of the clusters. We will determine such a potential for spherical clusters, in an electrostatic approximation, which allows for the use of the method of images. Note that in such approximation, the graphene sheet is an equipotential surface. Therefore, the Coulomb interaction due to the surface charge distribution of the clusters is perfectly screened by the surface charge distribution that it is generated on the graphene sheet. However, such induced charge distribution is spatially varying and it will thus correspond to a local variation of the Fermi level of graphene⁴⁴. Such variation will enter in the Dirac equation that describes the

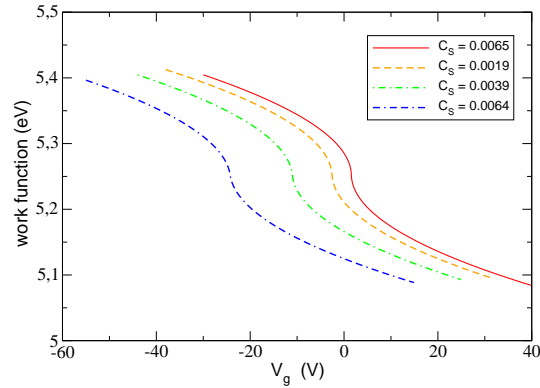


FIG. 4: Ionisation potential of cluster as a function of the applied gate voltage, for the Pt-3 sample, with coverages $c_S = 0.0065, 0.019, 0.039$ and 0.064 ML (rogb).

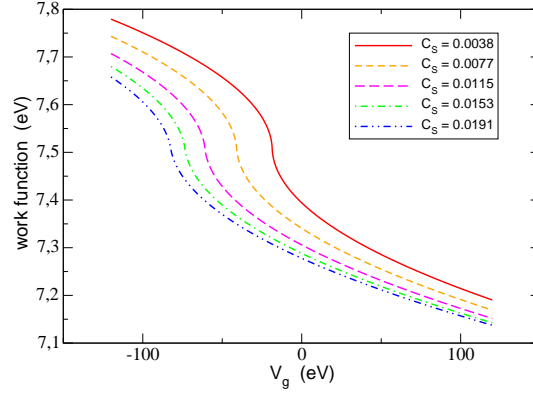


FIG. 5: Ionisation potential of cluster as a function of the applied gate voltage, for the Ti-1 sample, with coverages $C_S = 0.0038, 0.0077, 0.0115, 0.0153$ and 0.0191 ML (romgb).

low-energy properties of graphene as a scattering potential and will give rise to a variation of the conductivity. Note that the local variation of the Fermi energy due to a cluster is not a parameter of the model as in²³, but depends on the level of doping of graphene.

The clusters, of radius R , are placed at a distance $L > R$ above the graphene sheet. Each cluster possesses a charge $Q_S = -e\Delta N_S = -\frac{4}{3}\pi R^3 e \delta n_S$. We place the origin of the coordinate axis aligned with the centre of the spheres, such that the graphene sheet is located at $z = -L$. In the subspace $z \geq -L$, the electrostatic potential can be approximately described by the superposition

$$V(\mathbf{r}) = \sum_i v(\mathbf{r} - \mathbf{r}_i), \quad (25)$$

of the potentials due to the individual clusters, located at $\mathbf{r}_i = (x_i, y_i, 0)$.

In appendix B, we will show how $v(\mathbf{r})$ can be written in terms of a series of image charges, located in the cluster, and their images, located below the graphene plane. These charges depend on Q_S , R and L through a recursion relation. The displacement field in the subspace $z \geq -L$ is given by $\mathbf{D} = -\epsilon_0 \nabla V(\mathbf{r})$, whereas it is equal to $\mathbf{D} = -e \delta n_{Si} \mathbf{e}_z$ in the space between the graphene sheet and the Si layer. The discontinuity of its normal component at $z = -L$ determines the local density of charge $\sigma_g(x, y)$ in the graphene sheet. In terms of the density of carriers $\delta n_g(x, y) = -\sigma_g(x, y)/e$, one has

$$\delta n_g(x, y) = -\delta n_{Si} + \frac{\epsilon_0}{e} \left. \frac{\partial V(\mathbf{r})}{\partial z} \right|_{-L}, \quad (26)$$

where the derivative with respect to z is evaluated at the location of the graphene plane, $z = -L$. The spatial average of $\delta n_g(x, y)$ is given by equation (10). Averaging equation (26), we thus obtain $\left. \frac{\partial V(\mathbf{r})}{\partial z} \right|_{-L} = -\frac{e C_S v_S}{\epsilon_0 z_S A_c} \delta n_S$. Furthermore, one can write equation (26) as

$$\delta n_g(x, y) = \delta n_g + \frac{\epsilon_0}{e} \left[\left. \frac{\partial V(\mathbf{r})}{\partial z} \right|_{-L} - \overline{\left. \frac{\partial V(\mathbf{r})}{\partial z} \right|_{-L}} \right]. \quad (27)$$

The precise form of the local density of carriers depends on the location of the metallic clusters. However, assuming that one can treat clusters as independent entities, one has that in the neighbourhood of a given cluster, located at the origin of the coordinates, one can approximate (27) by

$$\delta n_g(x, y) \approx \delta n_g + \frac{\epsilon_0}{e} \left[\left. \frac{\partial v(\mathbf{r})}{\partial z} \right|_{-L} - \overline{\left. \frac{\partial v(\mathbf{r})}{\partial z} \right|_{-L}} \right], \quad (28)$$

where $v(\mathbf{r})$ is given by (B12). Using the previous results, one can also estimate that

$$\left. \frac{\partial v(\mathbf{r})}{\partial z} \right|_{-L} = -\frac{e C_S v_S}{\epsilon_0 z_S A_c N_c} \delta n_S, \quad (29)$$

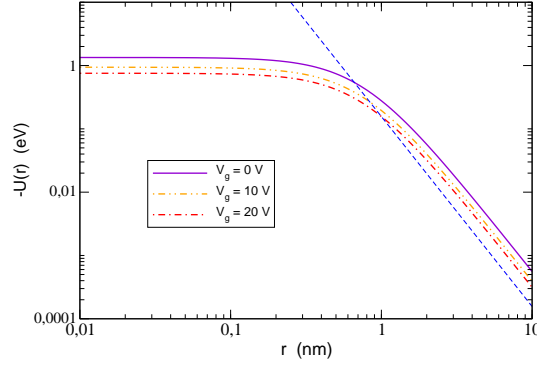


FIG. 6: Log-log plot of scattering potential due to clusters for Pt-1 sample with coverage $c_S = 0.025$ and applied voltages $V_G = 0, 10, 20$ V. The dashed line has slope -3 and is a guide to the eye.

where N_c is the number of clusters. Since such a number is supposed to be very large, this term is negligible and one has that

$$\delta n_g(x, y) \approx \delta n_g + \frac{\epsilon_0}{e} \left. \frac{\partial v(\mathbf{r})}{\partial z} \right|_{-L}. \quad (30)$$

Substituting equations (B12) and (B13) for $v(\mathbf{r})$ in (30) and expressing Q_S in terms of δn_S as above, one obtains the following series for $\delta n_g(r)$ ⁶³

$$\begin{aligned} \delta n_g(r) = & \delta n_g - \frac{2 R^3 \delta n_S \sqrt{L^2 - R^2}}{3 g(\lambda, 1)} \sum_{n=1}^{\infty} \frac{\lambda^n (1 + \lambda^{2n})}{(1 - \lambda^{2n})^2} \\ & \times \frac{1}{\left[r^2 + (L^2 - R^2) \left(\frac{1 + \lambda^{2n}}{1 - \lambda^{2n}} \right)^2 \right]^{3/2}}. \end{aligned} \quad (31)$$

where $\lambda = \frac{1}{R} (L - \sqrt{L^2 - R^2})$ and where $g(\lambda, 1)$ is given by (B7).

The local variation of the carrier density $\delta n_g(r)$ in graphene is related to the local variation of the Fermi energy $\Delta \varepsilon_F^g(r)$ through equation (18). Assuming that one is far from the neutrality point of graphene and that $\Delta \varepsilon_F^g(r)$ and $\Delta \varepsilon_F^g$ have the same sign, one has that the difference $U(r) = \Delta \varepsilon_F^g - \Delta \varepsilon_F^g(r)$ is given approximately by

$$\begin{aligned} U(r) \approx & \frac{\pi t^2 A_c \delta n_S R^3 \sqrt{L^2 - R^2}}{2 \sqrt{3} g(\lambda, 1) |\Delta \varepsilon_F^g|} \sum_{n=1}^{\infty} \frac{\lambda^n (1 + \lambda^{2n})}{(1 - \lambda^{2n})^2} \\ & \times \frac{1}{\left[r^2 + (L^2 - R^2) \left(\frac{1 + \lambda^{2n}}{1 - \lambda^{2n}} \right)^2 \right]^{3/2}}, \end{aligned} \quad (32)$$

where $\Delta \varepsilon_F^g$ is given by (22) and δn_S is given by (15). The function $U(r)$ is the electron scattering potential due to a single cluster and depends, in this approximation, on the cluster carrier density δn_S and also on the level of doping of graphene itself (through its dependence on $|\Delta \varepsilon_F^g|$). Note that $U(r)$ is attractive if $\delta n_S < 0$ (the cluster is doped with holes, as seen in experiment), as one would expect.

We can also compute from (31), for later use, the size of the region in graphene that contains a charge $-Q_S$ of equal magnitude to that of an individual clusters, in the case in which graphene is electron-doped (i.e. for $V > V_D$). We integrate equation (31) within the disk $r < R_S$, the region whose size we wish to calculate. We obtain after some cancellations, the following equation for R_S

$$\begin{aligned} R_S^2 = & \frac{4 R^3 \sqrt{L^2 - R^2} |\delta n_S|}{3 g(\lambda, 1) \delta n_g} \sum_{n=1}^{\infty} \frac{\lambda^n (1 + \lambda^{2n})}{(1 - \lambda^{2n})^2} \\ & \times \frac{1}{\left[R_S^2 + (L^2 - R^2) \left(\frac{1 + \lambda^{2n}}{1 - \lambda^{2n}} \right)^2 \right]^{1/2}}. \end{aligned} \quad (33)$$

This quantity should be compared with the average distance R_c between clusters, that can be simply defined through the relation $\pi R_c^2 = A_g/N_c = \frac{4\pi R^3 A_c z_S}{3c_S v_S}$, i.e. in terms of the average area per cluster. If one defines the ratio $\xi = R_S/R_c$ between these two quantities, one has, noting that the second fraction in the infinite sum of (33) can be simply approximated by R_S^{-1} if $R_S \gg L$, that ξ is approximately given by

$$\xi = \left(\sqrt{\frac{3}{4}} \frac{v_S^{3/2} \sqrt{L^2 - R^2}}{(A_c z_S R)^{3/2} g(\lambda, 1)} \sum_{n=1}^{\infty} \frac{\lambda^n (1 + \lambda^{2n})}{(1 - \lambda^{2n})^2} \right)^{1/3} \times \left(\frac{c_S^{3/2} |\delta n_S|}{\delta n_g} \right)^{1/3}, \quad (34)$$

where the first term is a constant for fixed L and R . The validity of the independent cluster approximation, assumed above when passing from (27) to (28), depends on the condition $\xi < 1^{64}$ being fulfilled.

The contribution of the metallic clusters to the resistivity of the sample of graphene can be easily computed within the FBA, once the scattering potential is known. Within the semi-classical theory⁴ based on the Boltzmann equation, the contribution of the clusters to the conductivity of the sample is given by

$$\sigma_{cl} = \frac{e^2 v_F k_F \tau_{cl}(k_F)}{\pi \hbar} \quad (35)$$

where $v_F = \frac{\sqrt{3} A_c / 2 t}{\hbar}$ is the Fermi velocity in graphene, $k_F = \frac{|\Delta \varepsilon_F^g|}{\hbar v_F}$ is the momentum of a quasi-particle at the Fermi surface of doped graphene, measured with respect to the Dirac point, and $\tau_{cl}(k_F)$ is the transport lifetime of a quasi-particle at the Fermi surface, due to the scattering with the metallic clusters. The expression above already accounts for the double spin and valley degeneracy (existence of two independent Dirac points). Equation (35) is known to apply as long as $k_F l_e \gg 1$, where l_e is the electron mean-free path. This condition holds in the diffusive regime where graphene is highly-doped (i.e. far away from the Dirac point) and for low-impurity concentration. The inverse of $\tau_{cl}(k_F)$ can be computed in the FBA, by the application of Fermi's Golden-Rule

$$\frac{1}{\tau_{cl}(k_F)} = \frac{2\pi}{\hbar} N_c \sum_{\mathbf{k}'} |\langle \mathbf{k}' | U(r) | \mathbf{k} \rangle|^2 \times (1 - \hat{\mathbf{k}}' \cdot \hat{\mathbf{k}}) \delta(\varepsilon_{\mathbf{k}'} - \varepsilon_{\mathbf{k}}), \quad (36)$$

where N_c is as above the number of clusters, i.e. the number of scattering centres, $|\mathbf{k}| = k_F$, $\varepsilon_{\mathbf{k}} = \hbar v_F |\mathbf{k}|$, $\varepsilon_{\mathbf{k}'} = \hbar v_F |\mathbf{k}'|$, $\hat{\mathbf{k}}$, $\hat{\mathbf{k}}'$ are the unit vectors in the direction of \mathbf{k} and \mathbf{k}' and $U(r)$ is given by (32).

In (36), one needs to take into account the spinorial nature of the wave-functions $|\mathbf{k}\rangle$, $|\mathbf{k}'\rangle$. The spinor $u_{\mathbf{k}}(\mathbf{r}) = \langle \mathbf{r} | \mathbf{k} \rangle$, which is normalized over the area A_g of the sample is given by

$$u_{\mathbf{k}}(\mathbf{r}) = \frac{1}{\sqrt{2A_g}} \begin{pmatrix} e^{-i\theta_{\mathbf{k}}/2} \\ \pm e^{i\theta_{\mathbf{k}}/2} \end{pmatrix} e^{i\mathbf{k} \cdot \mathbf{r}}, \quad (37)$$

where $\tan \theta_{\mathbf{k}} = k_y/k_x$. The \pm signs stand for states with the same momentum and opposite energies relative to the Dirac point. The expression for $u_{\mathbf{k}'}(\mathbf{r})$ is entirely analogous.

Substituting (37) and the analogous expression for $u_{\mathbf{k}'}(\mathbf{r})$ in (36), converting the summation over \mathbf{k}' into an integral, performing the integral over k' using the delta function and expressing $N_c/A_g = \frac{3c_S v_S}{4\pi R^3 z_S A_c}$, we obtain the following result in terms of an angular integral over the scattering angle $\phi = \theta_{\mathbf{k}'} - \theta_{\mathbf{k}}$,

$$\frac{1}{\tau_{cl}(k_F)} = \frac{\pi^2 c_S v_S v_F (\delta n_S)^2 R^3}{12 z_S A_c k_F g^2(\lambda, 1)} \int_0^{2\pi} d\phi \sin^2 \phi \times \left[\sum_{n=1}^{\infty} \frac{\lambda^n}{1 - \lambda^{2n}} e^{-\frac{2k_F \sqrt{L^2 - R^2} (1 + \lambda^{2n}) \sin(\phi/2)}{1 - \lambda^{2n}}} \right]^2. \quad (38)$$

The expression (38), as it stands, cannot be written in terms of elementary functions. However, the resulting integral is elementary if one can substitute the exponential functions in the infinite sum by 1, i.e. if their exponents are very small. The largest exponent is the one coming from the term with $n = 1$ and is equal to $2k_F L \sin(\phi/2)$. Thus, this approximation is valid if $k_F L \ll 1$. Since $\delta n_g = \pm \frac{k_F^2}{\pi}$, one can write the above condition as $|\delta n_g| \ll \frac{1}{\pi L^2}$. Taking $L \approx 1$

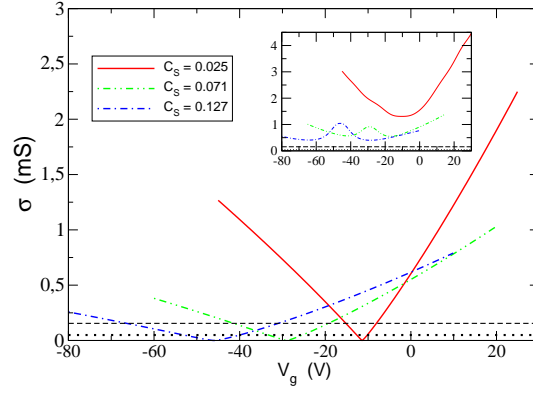


FIG. 7: Contribution to the conductivity of graphene sample due to Pt-clusters (Pt-1 sample) as function of the applied gate voltage, for the coverages $c_S = 0.025, 0.071$ and 0.127 ML (rgb), following the prediction of equation (39). The values of the two fitting parameters, the cluster radius $R = 0.6$ nm and distance $L = 0.85$ nm between the cluster center and the graphene sheet, are as given in Table I. Also shown are the minimal value for the conductivity $4e^2/(\pi h)$ predicted by the SCBA and the value of $4e^2/h$ measured by^{19,20}. Inset: contribution to the conductivity from the clusters as measured by²⁶.

nm, one obtains from this condition that $|\delta n_g| \ll 10^{13} - 10^{14} \text{ e/cm}^2$. This condition is obeyed for all experimentally applied voltages. Thus, substituting the resulting expression for $\tau_{cl}(k_F)$ in (35), one obtains

$$\sigma_{cl}(k_F) = \sigma_{min} \frac{6 z_S A_c |\delta n_g|}{\pi c_S v_S R^3 (\delta n_S)^2}, \quad (39)$$

where $\sigma_{min} = 4e^2/(\pi h)$ is the minimal conductivity of undoped graphene. Using the equations (22), (18) and (15) for $\Delta \varepsilon_F^g$, δn_g and δn_S in (39), with the relevant parameters in these equations taking the values as given in tables I, we plot below (see figure 7) the contribution to the conductivity of the graphene sample due to the clusters for the different coverages considered in²⁶ for their Pt-1 sample, as a function of the applied gate voltage V_G and as predicted by equation (39). Note the slight asymmetry of the curves with respect to the Dirac point, due to the variation of the carrier density δn_S of the cluster with the applied gate voltage.

One can also easily compute from (39) the contribution of the clusters to the mobility of the samples, defined as $\mu_{cl} = \sigma_{cl}/(e |\delta n_g|)$. One obtains

$$\mu_{cl}^{-1} = \frac{h \pi c_S}{32 e A_c} n_{amc} p_S^2, \quad (40)$$

where $p_S = v_S \delta n_S / z_S$ is the number of electrons per TM atom or doping efficiency.

The comparison of the result obtained in (39) with the experimental results of Pi et al. requires that we extract from their experimental data for the overall resistivity of the sample, the contribution coming solely from the metallic clusters, since there are other types of scatterers contributing to the resistivity even in an uncovered sample, as discussed in the introduction. Therefore, we make the following hypothesis regarding the dependence of the overall resistivity of a sample of graphene on the applied gate voltage V_G and on the metallic coverage c_S

$$\begin{aligned} \rho(V_G, c_S, n_i) = & \rho_{imp}(\delta n_g, n_i) + c_S \tilde{\rho}_{cl}(\delta n_g) \\ & + \rho_{MS}(\delta n_g, c_S, n_i), \end{aligned} \quad (41)$$

where n_i is the concentration of intrinsic impurities n_i in the sample. The function $\rho_{imp}(\delta n_g, n_i)$ is the contribution to the resistivity coming from the intrinsic impurities of the sample, which we take to be a sole function of the doping and of n_i . This function can be extracted from the measurements done at zero coverage by expressing $\rho(V_G, 0, n_i)$ as a function of δn_g , using equations (18) and (22) with $c_S = 0$. The second term is the contribution to the conductivity due to scattering by a single cluster and is therefore linear in c_S . Equation (39) is of this form, as we can always express δn_S in it in terms of δn_g through (15) and (18). However, this equation predicts an infinite resistivity due to the clusters at the Dirac point, since it assumes the system to be in the diffusive regime, an assumption that fails close to the Dirac point, as discussed above (see also¹⁶, where a similar situation occurs). Since the samples show a finite conductivity at the Dirac point and at finite coverage, we cannot take (39) as it stands. Instead, we write for

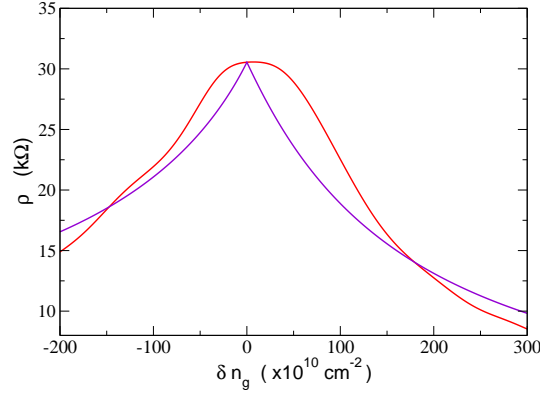


FIG. 8: Function $(\rho(V_G, c_S, n_i) - \rho(V_G, 0, n_i))/c_S$, as measured for the Pt-1 sample, expressed in terms of the doping level δn_g , for the coverage $c_S = 0.025$, plotted against the inverse of (42), in purple.

$\tilde{\sigma}_{cl} = \tilde{\rho}_{cl}^{-1}$, the ansatz

$$\tilde{\sigma}_{cl} = \tilde{\sigma}_{cl}^0 + \sigma_{min} \frac{6 z_S A_c |\delta n_g|}{\pi v_S R^3 (\delta n_S)^2}, \quad (42)$$

where $\tilde{\sigma}_{cl}^0$ is an extra contribution to the conductivity due to the clusters, which acts as an additional fitting parameter. Finally, $\rho_{MS}(\delta n_g, c_S, n_i)$ is the contribution to the resistivity due to multiple scattering events involving the metallic clusters, be it multiple scattering by a single cluster, scattering events involving different clusters, or events involving clusters and intrinsic impurities in graphene, and is a general function of c_S , δn_g and n_i .

If one were to assume that $\rho_{MS}(\delta n_g, c_S, n_i)$ were negligible, the function $(\rho(V_G, c_S, n_i) - \rho(V_G, 0, n_i))/c_S$, expressed in terms of δn_g , would be independent of the coverage c_S , i.e. it would be a universal curve. This is not the case for the metallic coverages considered by Pi et al, since these coverages are simply too large for multiple-scattering to be neglected, as will be shown below. In figure 8, we perform a fitting of the theory to the results obtained with sample Pt-1 at the lowest coverage studied, but the objective of such fitting is merely to show that with the parameters characterising the clusters as given in table I, the theoretical and experimental results have the same order of magnitude and show the same asymptotic behaviour. In purple, we plot the inverse of the function given by (42), with $\tilde{\sigma}_{cl}^0$ chosen so that the maximum of this curve and the maximum of the red curve coincide (this is the only free fitting parameter). We see that one is able to reproduce the asymptotic behaviour of the experimental curve at large doping. The same asymptotic behaviour is also observed at higher coverages, but the curves deviate significantly from the universal curve hypothesis in the neighbourhood of the Dirac point.

In order to understand the reason for the lack of agreement between the above theory and the experiments of²⁶, we consider the behaviour of the ratio ξ , introduced above, for the samples Pt-1 and Ti-1 (the behaviour observed for the sample Pt-3 is analogous to that of Pt-1). The plots are presented in figures 9 and 10. These plots indicate that, except for the lowest coverages, $\xi > 1$ in the whole range of doping displayed, and thus that the independent cluster approximation is unlikely to work for such high coverages. Note that this is purely a geometric effect, caused by the small size of the clusters. One can also write $R_c = \sqrt{\frac{n_{amc} A_c}{\pi c_S}} = a \sqrt{\frac{\sqrt{3} n_{amc}}{2 \pi c_S}}$, where $a = 2.46$ Å is the length of the primitive cell of graphene. For the lowest coverage studied in the two Pt samples that we analysed, i.e. $c_S = 0.0065$ ML for the Pt-3 sample, with $n_{amc} = 60$ atoms, $R_c \approx 12$ nm. In the case of the Ti-1 sample, $n_{amc} = 2$ atoms and for the lowest coverage studied $c_S = 0.0038$, $R_c \approx 3$ nm (for higher coverages, R_c is even smaller). Thus, in order to test the theory presented, the experiments performed would need to be repeated on samples presenting much lower concentrations of the deposited TM atoms (less than 1% for Pt-covered samples and less than 0.2% for Ti-covered samples). In addition, an appropriate characterisation of the clusters and their size distribution would also be required. With regard to the range of coverages studied experimentally by²⁶, one should also note that if one takes the doping level of graphene to be $\delta n_g \approx 10^{12} \text{ cm}^{-2}$, one has that $k_F \approx 10^6 \text{ cm}^{-1}$. Since $R_c \approx 10$ nm or less, $k_F R_c \sim 1$. This is yet another indication that a theory based on independent scattering centres is unlikely to work at this range of coverages. One should not expect that the contribution of multiple scattering to the resistivity $\rho_{MS}(\delta n_g, c_S, n_i)$ in (41) is a small quantity, in particular in the neighbourhood of the Dirac point²².

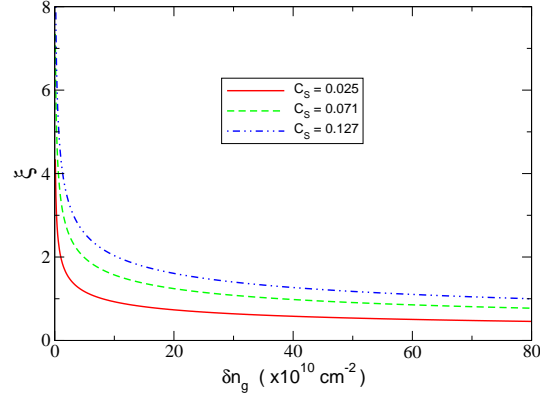


FIG. 9: Ratio ξ , as given by (34), expressed in terms of the doping level δn_g , for sample Pt-1, for the coverages $c_S = 0.025, 0.071$ and 0.127 ML (rgb).

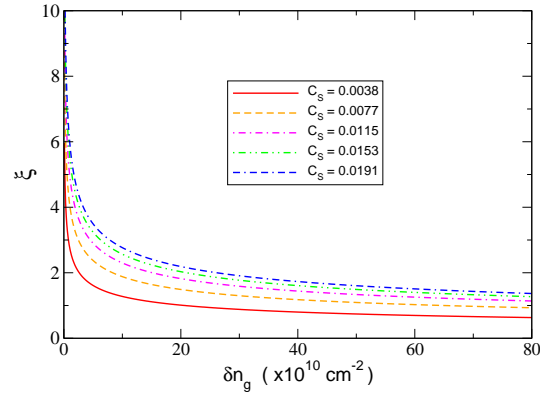


FIG. 10: Ratio ξ , as given by (34), expressed in terms of the doping level δn_g , for sample Ti-1, for the coverages $c_S = 0.0038, 0.0077, 0.0115, 0.0153$ and 0.0191 ML (romgb).

IV. CONCLUSIONS

In this paper, we performed a thermodynamic analysis of the problem of doping of graphene by TM clusters and computed the magnitude of the chemical interaction necessary to explain the electron doping of graphene by the transition metals Pt and Ti, the former having a bulk work function that is more than 1 eV larger than the work function of graphene. We have shown that the enhancement of such interaction with respect to the case studied in^{35,36} is due to the finite size of the TM clusters. We have also determined the scattering potential induced in a graphene sheet by spherical TM clusters and its contribution to the resistivity of the sample in the FBA. We have shown that regime of coverages for which the transport theory presented is likely to have a predictive power is below those coverages considered in the experiments of Pi et al. and thus one would need to repeat such experiments in these regimes in order to fully test such a theory.

Acknowledgements: We acknowledge helpful discussions with K. McCreary, R. Kawakami, P. Fulde, A. Ferreira and E. Lage. J.E.S. acknowledges support by FCT under Grant No.PTDC/FIS/64404/2006 and by the Visitors Program of MPIPks at the different stages of this work. A.H.C.N. acknowledges support from the DOE grant DE-FG02-08ER46512 and the ONR grant MURI N00014-09-1-1063.

Appendix A: Calculation of a cluster's ionisation potential based on a thermodynamic argument

One can also determine the ionisation potential of a cluster from thermodynamic considerations. One starts by considering the expression for the energy (4) in the case of a single cluster ($N_c = 1$). Since the expression (4) is valid for a system that is neutral, the extraction of a charge $-e$ from the cluster requires this charge to be replaced in the graphene sheet. As discussed in appendix B, the placement of such a charge in the graphene sheet can be pictured as the withdrawal of the image charge $+e$ of the cluster charge $-e$, as the latter one is removed to infinity. Thus, one has from (4) that

$$\begin{aligned} I_S - W_g &= \mathcal{E}(N_S - 1, N_g + 1, N_{Si}) - \mathcal{E}(N_S, N_g, N_{Si}) \\ &= -\bar{\mu}_S + \bar{\mu}_g + e(D_S - D_g) \\ &\quad - \frac{e^2}{C_S} (N_S - N_S^0) + \frac{e^2}{2C_S}. \end{aligned} \quad (\text{A1})$$

Provided that the area of the graphene sheet is large, $W_g = -\bar{\mu}_g + eD_g$, and thus

$$I_S = -\bar{\mu}_S + eD_S - \frac{e^2}{C_S} (N_S - N_S^0) + \frac{e^2}{2C_S}. \quad (\text{A2})$$

One can consider the difference in the value of the ionisation potential I_S and the ionisation potential I_S^0 in a situation where the cluster is placed very far away from the graphene sheet. One has

$$\begin{aligned} I_S - I_S^0 &= -\Delta\bar{\mu}_S + e(D_S - D_S^0) - e^2 \left(\frac{1}{C_S} - \frac{1}{C_S^0} \right) \Delta N_S \\ &\quad + \frac{e^2}{2} \left(\frac{1}{C_S} - \frac{1}{C_S^0} \right). \end{aligned} \quad (\text{A3})$$

Note that D_S^0 is not identical to D_B , due to the finite size of the cluster. In appendix B, we will show how the last two terms of (A3) are obtained using the method of images to compute I_S for the case of a spherical cluster.

Finally, one can use the equilibrium condition (6) to write (A1) as

$$I_S = W_g + \frac{e^2}{2C_S} = -\bar{\mu}_g + eD_g + \frac{e^2}{2C_S}. \quad (\text{A4})$$

As stated above, one can explicitly compute the capacitance of a spherical cluster of radius R , whose centre lies at a distance $L > R$, see appendix B. In this case, and in the limit $R, L \rightarrow \infty$, with $\eta = R/2L$ finite, i.e. for graphene adsorbed on the bulk transition metal, as considered by^{35,36}, $C_S \rightarrow \infty$, and the transition metal ionisation potential and the work-function of graphene become equal at equilibrium, as one would expect (in this case, I_S would just reduce to the TM work-function). For a spherical metal cluster of finite radius, there is an extra contribution to its ionisation potential, coming from the effect of the image charge, already present in the case of an isolated spherical cluster⁶⁰. This is the last term of the rhs of equation (A4).

One can also compute the cluster's electron affinity A_S using the above argument. In this case, one is withdrawing an electron from an over-charged cluster and delivering it to the graphene sheet. One has

$$\begin{aligned} A_S - W_g &= \mathcal{E}(N_S, N_g, N_{Si}) - \mathcal{E}(N_S + 1, N_g - 1, N_{Si}) \\ &= -\bar{\mu}_S + \bar{\mu}_g + e(D_S - D_g) \\ &\quad - \frac{e^2}{C_S} (N_S - N_S^0) - \frac{e^2}{2C_S} = -\frac{e^2}{2C_S}, \end{aligned} \quad (\text{A5})$$

where we have again used the equilibrium condition (6). Note, in closing, that $W_g = \frac{1}{2}(I_S + A_S)$, as one would expect.

Appendix B: Calculation of the electrostatic contribution to the ionisation potential of a spherical cluster close to a grounded plane and of the electrostatic potential created by it

We will now compute the ionisation potential of a system composed by a single metallic spherical cluster and a grounded graphene plane using the method of images, by considering the electrostatic work necessary to extract a single electron from the cluster. These considerations will also allow us to write an explicit expression for the system's

capacitance and for the electrostatic potential created by the cluster in the upper-half space, i.e. the quantity $v(\mathbf{r})$, introduced in section III, necessary to determine the scattering potential of carriers in graphene due to the presence of the spherical cluster.

As above, the sphere contains a total charge Q_S and we will extract a charge q_0 from it, leaving a total charge $Q_S - q_0$ in it. The charge q_0 is the elementary charge $-e$. The ionisation potential of this system is the energy necessary to displace q_0 from a distance d away from the surface of the sphere to infinity. The distance d at which one begins to perform work to extract the charge q_0 is a regularisation parameter necessary to take into account the singular nature of the Coulomb interaction, but one can also interpret it physically as being the distance beyond which quantum corrections to the Coulomb law become negligible.

The conditions of the problem are as described in section III. In order to determine the force on q_0 as it is displaced from $z = d + R$ to $z = \infty$, one needs to determine the potential created by the presence of the sphere and of the plane at the position of the charge. Such potential can be determined by the method of images, as shown below.

In the absence of a conducting plane, the solution of the problem is trivial. If q_0 is located at $z = z_0$, one places an image charge of magnitude $q_1 = -q_0 R/z_0$ in the interior of the sphere at $z_1 = R^2/z_0$ and an image charge $q_2 = Q_S - q_0 - q_1$ at the centre of the sphere. These three charges guaranty that the surface of the sphere is equipotential and that the sphere has an overall charge $Q_S - q_0$ in it. In the presence of a grounded plane, these three charges no longer guaranty that the surface $z = -L$ is an equipotential. We therefore take q_2 to have an arbitrary value for the moment and consider three image charges $q_3 = -q_0$ at $z_3 = -(2L + z_0)$, $q_4 = -q_1$ at $z_4 = -(2L + z_1)$ and $q_5 = -q_2$ at $z_5 = -2L$, located below the plane. These three charges will guaranty that the plane $z = -L$ is an equipotential. However, the surface of the sphere is no longer an equipotential. We therefore place three image charges in the interior of the sphere, $q_6 = -q_3 \frac{R}{|z_3|} = \frac{q_0}{2L+z_0}$ at $z_6 = -\frac{R^2}{|z_3|} = -\frac{R^2}{2L+z_0}$, $q_7 = -q_4 \frac{R}{|z_4|} = q_1 \frac{R}{2L+z_1}$ at $z_7 = -\frac{R^2}{|z_4|} = -\frac{R^2}{2L+z_1}$ and $q_8 = -q_5 \frac{R}{|z_5|} = q_2 \frac{R}{2L}$ at $z_8 = -\frac{R^2}{|z_5|} = -\frac{R^2}{2L}$. In order to balance the potential at the surface of the plane, we now need to place three image charges below the plane, followed by three image charges inside the sphere and so on *ad infinitum*. The arguments above suggest that the recurrence relation between the charges inside the sphere is given by

$$\begin{cases} q_{6(n+1)+\alpha} = q_{6n+\alpha} \frac{R}{2L+z_{6n+\alpha}} \\ z_{6(n+1)+\alpha} = -\frac{R^2}{2L+z_{6n+\alpha}} \end{cases} \quad (B1)$$

where $n \geq 0$ and $\alpha = 0, 1, 2$. The recurrence relation between the charges located inside the sphere and below the plane is simpler, $q_{6n+3+\alpha} = -q_{6n+\alpha}$, $z_{6n+3+\alpha} = -(2L + z_{6n+\alpha})$.

The charge on the sphere is given by

$$\begin{aligned} Q_S &= q_0 + q_1 + q_2 + q_6 + q_7 + q_8 + q_{12} + q_{13} + q_{14} + \dots \\ &= \sum_{n=0, \alpha}^{\infty} q_{6n+\alpha}. \end{aligned} \quad (B2)$$

This equation determines the charge q_2 in terms of Q_S and q_0 . Let us rewrite the recursion relation above in a slightly different form. We define $\pi_n^\alpha = q_{6n+\alpha}$, $w_n^\alpha = \frac{z_{6n+\alpha}}{2L}$ and $\eta = \frac{R}{2L} < \frac{1}{2}$. We have

$$\begin{cases} \pi_{n+1}^\alpha = \pi_n^\alpha \frac{\eta}{1+w_n^\alpha} \\ w_{n+1}^\alpha = -\frac{\eta^2}{1+w_n^\alpha} \end{cases} \quad (B3)$$

We now define $u_n^\alpha = \frac{1}{\pi_n^\alpha}$ ⁶⁵. It is easy to see from (B3) that we have $u_{n+1}^\alpha = u_n^\alpha \frac{1+w_n^\alpha}{\eta}$ and $u_{n-1}^\alpha = u_n^\alpha \frac{\eta}{1+w_{n-1}^\alpha}$. Adding the two equations and using the recursion relation for w_n^α , we have

$$u_{n+1}^\alpha + u_{n-1}^\alpha = \frac{u_n^\alpha}{\eta}. \quad (B4)$$

This is a linear recursion relation, with solution $u_n^\alpha = A_+^\alpha s_+^n + A_-^\alpha s_-^n$, where s_\pm are the solutions of the quadratic equation $\eta(s_\pm^2 + 1) - s_\pm = 0$, which are given by $s_\pm = \frac{1}{2\eta} \pm \frac{\sqrt{1-4\eta^2}}{2\eta}$, with $s_+ s_- = 1$ and $s_+ > 1, s_- < 1$. For definitiveness, we will call $s_- = \lambda, s_+ = \lambda^{-1}$. In this case, we have

$$\begin{cases} u_n^\alpha = A_+^\alpha \lambda^{-n} + A_-^\alpha \lambda^n \\ w_n^\alpha = -\frac{\eta(A_+^\alpha \lambda^{1-n} + A_-^\alpha \lambda^{n-1})}{A_+^\alpha \lambda^{-n} + A_-^\alpha \lambda^n} \end{cases}, \quad (B5)$$

where we have made use of the relation $\eta(\lambda^{-1} + \lambda) = 1$. The value of the coefficients A_{\pm}^{α} is determined from the known values of $u_0^{\alpha}, w_0^{\alpha}$, namely $u_0^0 = q_0^{-1}$, $w_0^0 = w_0 = z_0/2L$, $u_0^1 = -q_0^{-1} \frac{w_0}{\eta}$, $w_0^1 = \frac{\eta^2}{w_0}$ and $u_0^2 = q_2^{-1}$, $w_0^2 = 0$. One obtains $A_+^0 = \frac{1}{q_0\eta} \frac{w_0 + \eta\lambda^{-1}}{\lambda^{-1} - \lambda}$, $A_-^0 = -\frac{1}{q_0\eta} \frac{w_0 + \eta\lambda}{\lambda^{-1} - \lambda}$, $A_+^1 = -\frac{1}{q_0\eta\lambda} \frac{w_0 + \eta\lambda}{\lambda^{-1} - \lambda}$, $A_-^1 = \frac{\lambda}{q_0\eta} \frac{w_0 + \eta\lambda^{-1}}{\lambda^{-1} - \lambda}$ and $A_+^2 = \frac{1}{q_2} \frac{\lambda^{-1}}{\lambda^{-1} - \lambda}$, $A_-^2 = -\frac{1}{q_2} \frac{\lambda}{\lambda^{-1} - \lambda}$. Substituting these relations in equation and equation (B5) in equation (B2), one obtains for q_2 the following result

$$q_2(\lambda, \xi) = \frac{Q_S - q_0}{\lambda^{-1} - \lambda} g^{-1}(\lambda, 1) - \frac{q_0(1 - \xi)}{\lambda^{-1} - \lambda} \times (g(\lambda, \xi) - \xi^{-1} g(\lambda, \xi^{-1})) g^{-1}(\lambda, 1), \quad (\text{B6})$$

where $\xi = \frac{w_0 + \eta\lambda}{w_0 + \eta\lambda^{-1}} < 1$ and⁶⁶

$$g(\lambda, \xi) = \sum_{n=1}^{\infty} \frac{\lambda^n}{1 - \xi\lambda^{2n}}. \quad (\text{B7})$$

Note that one can use this result to compute the capacitance of the system composed by the sphere and the plane. For such a calculation, one takes $q_0 = 0$ (or $w_0 \rightarrow \eta$, i.e. $\xi \rightarrow \lambda$). The charge of the sphere is Q_S and the potential at its surface is given by $V_S = \frac{q_2}{4\pi\epsilon_0 R}$. Hence, the capacitance $C_S = Q_S/V_S$ is, using (B6) with $q_0 = 0$, given by

$$C_S = 4\pi\epsilon_0 R (1 - \lambda^2) g(\lambda, 1)/\lambda. \quad (\text{B8})$$

In terms of η , the first few terms of this series are $C_S = 4\pi\epsilon_0 R \left(1 + \eta + \frac{\eta^2}{1 - \eta^2} + \dots\right)$.

The potential created by the image charges along the z -axis ($z \geq R$) is given by

$$V_{im}(z, z_0) = \frac{1}{4\pi\epsilon_0} \left\{ \sum_{[n, \alpha]}^{\infty} \frac{q_{6n+\alpha}}{z - z_{6n+\alpha}} - \sum_{n, \alpha}^{\infty} \frac{q_{6n+\alpha}}{z + 2L + z_{6n+\alpha}} \right\}, \quad (\text{B9})$$

where we have used the recursion relation between the image charges on the plane and those on the sphere, and where the notation $[n, \alpha]$ indicates that the term $n = 0, \alpha = 0$ (potential created by q_0) is absent from the first sum. The notation $V_{im}(z, z_0)$ indicates that the potential depends on z_0 through its dependence on the position and magnitude of the image charges. Expressing $q_{6n+\alpha}$ in terms of u_n^{α} and $z_{6n+\alpha}$ in terms of w_n^{α} and using the rescaled variable $w = z/2L$, we have that $V_{im}(w, w_0)$ is given by

$$V_{im}(w, w_0) = \frac{1}{8\pi\epsilon_0 L} \left\{ \sum_{[n, \alpha]}^{\infty} \frac{1}{u_n^{\alpha}(w - w_n^{\alpha})} - \sum_{n, \alpha}^{\infty} \frac{1}{u_n^{\alpha}(w + 1 + w_n^{\alpha})} \right\}. \quad (\text{B10})$$

Substituting the recursion relations given by (B5) above, we obtain for $\mathcal{U}_{im}(w, w_0) = 8\pi\epsilon_0 L V_{im}(w, w_0)$

$$\mathcal{U}_{im}(w, w_0) = \sum_{[n, \alpha]}^{\infty} \frac{1}{A_+^{\alpha} \lambda^{-n}(w + \eta\lambda) + A_-^{\alpha} \lambda^n(w + \eta\lambda^{-1})} - \sum_{n, \alpha}^{\infty} \frac{1}{A_+^{\alpha} \lambda^{-n}(w + \eta\lambda^{-1}) + A_-^{\alpha} \lambda^n(w + \eta\lambda)}. \quad (\text{B11})$$

The potential $v(\mathbf{r})$ created by the cluster on the subspace $z \geq -L$, when its charge is equal to Q_S , which was introduced in section III, can also be computed in a manner analogous to $V_{im}(z, z_0)$. In this case one sets $q_0 = 0$, as in the calculation of the capacitance, in the recursion relation (B5). One is now interested in the dependence of $v(\mathbf{r})$ both on z and on the radial coordinate r along the xy plane.

This potential is given by

$$v(\mathbf{r}) = \frac{1}{4\pi\epsilon_0} \sum_{n=0}^{\infty} \left(\frac{q_{6n+2}}{[r^2 + (z - z_{6n+2})^2]^{1/2}} - \frac{q_{6n+2}}{[r^2 + (z + 2L + z_{6n+2})^2]^{1/2}} \right), \quad (\text{B12})$$

where $r = \sqrt{x^2 + y^2}$ is the distance in the graphene sheet and where q_{6n+2} and z_{6n+2} are given by

$$\begin{cases} q_{6n+2} = \frac{Q_S g^{-1}(\lambda, 1)}{\lambda^{-(n+1)} - \lambda^{(n+1)}} \\ z_{6n+2} = -R \frac{\lambda^{-n} - \lambda^n}{\lambda^{-(n+1)} - \lambda^{(n+1)}} \end{cases}. \quad (\text{B13})$$

One can now use (B11) to compute the ionisation potential of the system cluster-graphene plane. This quantity is equal to the work of the external force necessary to transport the charge q_0 from $z = R+d$ up to $z = \infty$ quasi-statically, i.e. $I_S(d) = \int_{R+d}^{\infty} dz_0 F_{ext}(z_0)$, where $F_{ext}(z_0) = \frac{q_0}{16\pi\epsilon_0 L^2} \frac{\partial \mathcal{U}_{im}}{\partial w} |_{w=w_0}$.

Substituting the values A_{\pm}^{α} obtained above in (B11) and performing the derivative of $\mathcal{U}_{im}(w, w_0)$ with respect to w at $w = w_0$, one obtains the rather lengthy expression for $f_{ext}(w_0) = \frac{1}{\eta(\lambda^{-1} - \lambda)} \frac{\partial \mathcal{U}_{im}}{\partial w} |_{w=w_0}$,

$$\begin{aligned} f_{ext}(w_0) = & q_0 \sum_{n=0}^{\infty} \frac{(w_0 + \eta\lambda^{-1})\lambda^{-n} - (w_0 + \eta\lambda)\lambda^n}{[(w_0 + \eta\lambda^{-1})^2\lambda^{-n} - (w_0 + \eta\lambda)^2\lambda^n]^2} \\ & + q_0 \sum_{n=1}^{\infty} \frac{(w_0 + \eta\lambda)\lambda^{-n} - (w_0 + \eta\lambda^{-1})\lambda^n}{[(w_0 + \eta\lambda)^2\lambda^{-n} - (w_0 + \eta\lambda^{-1})^2\lambda^n]^2} \\ & - q_0 \sum_{n=1}^{\infty} \frac{(w_0 + \eta\lambda^{-1})\lambda^{-n} - (w_0 + \eta\lambda)\lambda^n}{[(w_0 + \eta\lambda^{-1})(w_0 + \eta\lambda)(\lambda^{-n} - \lambda^n)]^2} \\ & - q_0 \sum_{n=1}^{\infty} \frac{(w_0 + \eta\lambda)\lambda^{-n} - (w_0 + \eta\lambda^{-1})\lambda^n}{[(w_0 + \eta\lambda^{-1})(w_0 + \eta\lambda)(\lambda^{-n} - \lambda^n)]^2} \\ & + q_2 \sum_{n=1}^{\infty} \frac{\lambda^{-n} - \lambda^n}{[(w_0 + \eta\lambda^{-1})\lambda^{-n} - (w_0 + \eta\lambda)\lambda^n]^2} \\ & - q_2 \sum_{n=1}^{\infty} \frac{\lambda^{-n} - \lambda^n}{[(w_0 + \eta\lambda)\lambda^{-n} - (w_0 + \eta\lambda^{-1})\lambda^n]^2}. \end{aligned} \quad (\text{B14})$$

This expression has to be integrated so as to obtain the ionisation potential $I_S(d) = \frac{q_0 \sqrt{L^2 - R^2}}{8\pi\epsilon_0 L^2} \int_{\eta+\gamma}^{\infty} dw_0 f_{ext}(w_0)$, where $\gamma = d/2L$. It is more convenient to express this integral in terms of the variable ξ introduced above. The result is

$$\begin{aligned} I_S(d) = & \frac{q_0^2}{8\pi\epsilon_0 \sqrt{L^2 - R^2}} \int_{1/\delta}^1 d\xi (1 - \xi) \\ & \times \left[\sum_{n=0}^{\infty} \frac{\lambda^n (1 - \xi\lambda^{2n})}{(1 - \xi^2\lambda^{2n})^2} \right. \\ & \left. + \frac{1}{\xi^3} \sum_{n=1}^{\infty} \frac{\lambda^n (1 - \xi^{-1}\lambda^{2n})}{(1 - \xi^{-2}\lambda^{2n})^2} \right] \\ & + \frac{q_0^2 g(\lambda, 1)}{8\pi\epsilon_0 \sqrt{L^2 - R^2}} \int_{1/\delta}^1 d\xi \left(1 - \frac{1}{\xi^2} \right) \\ & + \frac{q_0}{4\pi\epsilon_0 R} \int_{1/\delta}^1 d\xi q_2(\lambda, \xi) \left[\sum_{n=1}^{\infty} \frac{\lambda^n (1 - \lambda^{2n})}{(1 - \xi\lambda^{2n})^2} \right. \\ & \left. - \frac{1}{\xi^2} \sum_{n=1}^{\infty} \frac{\lambda^n (1 - \lambda^{2n})}{(1 - \xi^{-1}\lambda^{2n})^2} \right], \end{aligned} \quad (\text{B15})$$

where $q_2(\lambda, \xi)$ is given in equation (B6), where we have also introduced $g(\lambda, \xi)$ and where $\delta = \frac{\eta + \gamma + \eta\lambda^{-1}}{\eta + \gamma + \eta\lambda} > 1$ and $\delta < \lambda^{-1}$, being equal to it in when $d = 0$. The first term in this expression can be integrated using the following identity

$$\begin{aligned} & \frac{1}{2(1-\xi)} \frac{\partial}{\partial \xi} \{ (1-\xi)^2 [g(\lambda, \xi^2) + \xi^{-2} g(\lambda, \xi^{-2})] \} = \\ & - \left[\sum_{n=1}^{\infty} \frac{\lambda^n (1 - \xi \lambda^{2n})}{(1 - \xi^2 \lambda^{2n})^2} + \frac{1}{\xi^3} \sum_{n=1}^{\infty} \frac{\lambda^n (1 - \xi^{-1} \lambda^{2n})}{(1 - \xi^{-2} \lambda^{2n})^2} \right]. \end{aligned} \quad (\text{B16})$$

The second term involves a trivial integral. As for the third term, it can also be integrated if one notes that the following identity holds

$$\begin{aligned} & -\frac{\partial}{\partial \xi} \{ (1-\xi) [g(\lambda, \xi) - \xi^{-1} g(\lambda, \xi^{-1})] \} = \\ & \sum_{n=1}^{\infty} \frac{\lambda^n (1 - \lambda^{2n})}{(1 - \xi \lambda^{2n})^2} - \frac{1}{\xi^2} \sum_{n=1}^{\infty} \frac{\lambda^n (1 - \lambda^{2n})}{(1 - \xi^{-1} \lambda^{2n})^2}. \end{aligned} \quad (\text{B17})$$

Substituting these results and (B6) in (B15), performing the resulting integrals and putting $q_0 = -e$, one obtains after some trivial manipulations, the final result

$$\begin{aligned} I_S(d) = & \frac{e^2}{16\pi\epsilon_0(L+R+d)} \\ & + \frac{e^2 \sqrt{L^2 - R^2}}{4\pi\epsilon_0 [L+R+d - \sqrt{L^2 - R^2}]^2} \\ & \times [g(\lambda, \delta^2) + \delta^{-2} g(\lambda, \delta^{-2})] \\ & - \frac{e^2 \sqrt{L^2 - R^2} g(\lambda, 1)}{2\pi\epsilon_0 [d^2 + 2(R+L)(R+d)]} \\ & + \frac{(e^2 + e Q_S) g^{-1}(\lambda, 1)}{4\pi\epsilon_0 [L+R+d - \sqrt{L^2 - R^2}]} \\ & \times [g(\lambda, \delta) - \delta^{-1} g(\lambda, \delta^{-1})] \\ & - \frac{e^2 \sqrt{L^2 - R^2} g^{-1}(\lambda, 1)}{4\pi\epsilon_0 [L+R+d + \sqrt{L^2 - R^2}]^2} \\ & \times [g(\lambda, \delta) - \delta^{-1} g(\lambda, \delta^{-1})]^2. \end{aligned} \quad (\text{B18})$$

In the limit $L \rightarrow \infty$, we are left with an isolated charged cluster. We obtain from (B18) the known result

$$\begin{aligned} I_S^0(d) = & \frac{e^2}{4\pi\epsilon_0} \left(\frac{R}{2d(d+2R)} + \frac{1}{R+d} - \frac{R}{2(R+d)^2} \right) \\ & + \frac{e Q_S}{4\pi\epsilon_0(R+d)}. \end{aligned} \quad (\text{B19})$$

The only term in (B18) that is singular in the limit $d \rightarrow 0$ is the first term of the series $g(\lambda, \delta^2)$ ($\delta \rightarrow \lambda^{-1}$ in this limit). Moreover, for finite d , this term is equal to the corresponding singular term in (B19). Thus, $\Phi(d) = I_S(d) - I_S^0(d)$ is a regular function in the limit $d \rightarrow 0$. It equals

$$\Phi(0) = e Q_S \left(\frac{1}{C_S} - \frac{1}{C_S^0} \right) + \frac{e^2}{2} \left(\frac{1}{C_S} - \frac{1}{C_S^0} \right), \quad (\text{B20})$$

with $C_S^0 = 4\pi\epsilon_0 R$ and where C_S is given by (B8). Since $Q_S = -e \Delta N_S$, we see that the result (B20) is equal to the last two terms of (A2), which correspond to the electrostatic contribution to I_S , the only one considered here. This justifies the statement made in appendix A.

* Electronic address: jesantos@pks.mpg.de

- ¹ K. S. Novoselov, A. K. Geim, S. V. Morozov, D. Jiang, Y. Zhang, S. V. Dubonos, I. V. Grigorieva and A. A. Firsov, *Science* **306**, 666 (2004).
- ² K. S. Novoselov, D. Jiang, T. Booth, V.V. Khotkevich, S. M. Morozov and A. K. Geim, *PNAS* **102**, 10451 (2005).
- ³ A.H. Castro Neto, F. Guinea, N.M.R. Peres, K.S. Novoselov and A.K. Geim, *Rev. Mod. Phys.* **81**, 109 (2009).
- ⁴ D. Abergel, V. Apalkov, J. Berashevich, K. Ziegler and T. Chakrabortya, *Adv. Phys.* **59**, 261 (2010).
- ⁵ L. X. WangZhi and K. Mullen, *Nano Lett.* **8**, 323 (2008).
- ⁶ P. Blake, P. D. Brimicombe, R. R. Nair, T. J. Booth, D. Jiang, F. Schedin, L. A. Ponomarenko, S. V. Morozov, H. F. Gleeson, E. W. Hill, A. K. Geim and K. S. Novoselov, *Nano Lett.* **8**, 1704 (2008).
- ⁷ F. Schedin, A. K. Geim, S. V. Morozov, D. Jiang, E. H. Hill, P. Blake and K. S. Novoselov, *Nature Materials* **6**, 652 (2007).
- ⁸ X. Wang, Y. Ouyang, X. Li, H. Wang, J. Guo and H. Dai, *Phys. Rev. Lett.* **100**, 206803 (2008).
- ⁹ N. Schon and T. Ando, *J. Phys. Soc. Jpn.* **67**, 2421 (1998).
- ¹⁰ Y. Zheng and T. Ando, *Phys. Rev. B* **65**, 245420 (2002).
- ¹¹ P. M. Ostrovsky, I. V. Gornyi and A. D. Mirlin, *Phys. Rev. B* **74**, 235443 (2006).
- ¹² N. M. R. Peres, F. Guinea, and A. H. Castro Neto, *Phys. Rev. B* **73**, 125411 (2006).
- ¹³ T. Stauber, N. M. R. Peres, and A. H. Castro Neto, *Phys. Rev. B* **78**, 085418 (2008).
- ¹⁴ M. Katsnelson, *Eur. Phys. J. B* **51**, 157 (2006).
- ¹⁵ B. Dóra, K. Ziegler and P. Thalmeier, *Phys. Rev. B* **77**, 115422 (2008).
- ¹⁶ N. Leconte, J. Moser, P. Ordejón, H. Tao, A. Lherbier, A. Bachtold, F. Alsina, C. M. Sotomayor Torres, J. C. Charlier and S. Roche, *ACS Nano* **4**, 4033 (2010).
- ¹⁷ A. Lherbier, B. Biel, Y. M. Niquet and S. Roche, *Phys. Rev.* **100**, 036803 (2008).
- ¹⁸ A. Lherbier, S. M. -M. Dubois, X. Declerck, S. Roche, Y. M. Niquet and J. C. Charlier, *Phys. Rev. Lett.* **106**, 046803 (2011).
- ¹⁹ A. K. Geim and K. S. Novoselov, *Nature Mater.* **6**, 183 (2007).
- ²⁰ Y. W. Tan, Y. Zhang, K. Bolotin, Y. Zhao, S. Adam, E. H. Hwang, S. Das Sarma, H. L. Stormer and P. Kim, *Phys. Rev. Lett.* **99**, 246803 (2007).
- ²¹ A. Lherbier, X. Blase, Y. M. Niquet, F. Triozon and S. Roche, *Phys. Rev. Lett.* **101**, 036808 (2008).
- ²² A. Ferreira, J. Viana-Gomes, J. Nilsson, E. R. Mucciolo, N. M. R. Peres and A. H. Castro Neto, *Phys. Rev. B* **83**, 165402 (2011).
- ²³ M. I. Katsnelson and F. Guinea and A. K. Geim, *Phys. Rev. B* **79**, 195426 (2009).
- ²⁴ L. A. Ponomarenko, R. Yang, T. M. Mohiuddin, M. I. Katsnelson, K. S. Novoselov, S. V. Morozov, A. A. Zhukov, F. Schedin, E. W. Hill and A. K. Geim, *Phys. Rev. Lett.* **102**, 206603 (2009).
- ²⁵ N. M. R. Peres, *Rev. Mod. Phys.* **82**, 2673 (2010).
- ²⁶ K. Pi, K. M. McCreary, W. Bao, Wei Han, Y. F. Chiang, Yan Li, S.-W. Tsai, C. N. Lau and R. K. Kawakami, *Phys. Rev. B* **80**, 075406 (2009).
- ²⁷ S. Marchini, S. Günther, and J. Wintterlin, *Phys. Rev. B* **76**, 075429 (2007).
- ²⁸ A. L. Vázquez de Parga, F. Calleja, B. Borca, M. C. G. Passeggi, J. J. Hinarejos, F. Guinea, and R. Miranda, *Phys. Rev. Lett.* **100**, 056807 (2008).
- ²⁹ P. W. Sutter, J. I. Flege, and E. A. Sutter, *Nature Mater.* **7**, 406 (2008).
- ³⁰ A. B. Preobrazjenski, M. L. Ng, A. S. Vinogradov and N. Martensson, *Phys. Rev. B* **78**, 073401 (2008).
- ³¹ K. T. Chan, J. B. Neaton and M. L. Cohen, *Phys. Rev. B* **77**, 235430 (2008).
- ³² Y. Mao, J. Yuan and J. Zhang, *J. Phys. Cond. Mat.* **20**, 115209 (2008).
- ³³ B. Wang, M. L. Bocquet, S. Marchini, S. Günther and J. Wintterlin, *Phys. Chem. Chem. Phys.* **10**, 3530 (2008).
- ³⁴ D. Jiang, M. Du and S. Dai, *J. Chem. Phys.* **130**, 074705 (2009).
- ³⁵ G. Giovannetti, P. A. Khomyakov, G. Brocks, V. M. Karpan, J. van den Brink and P. J. Kelly, *Phys. Rev. Lett.* **101**, 026803 (2008).
- ³⁶ P. A. Khomyakov, G. Giovannetti, P. C. Rusu, G. Brocks, J. van den Brink and P. J. Kelly, *Phys. Rev. B* **79**, 195425 (2009).
- ³⁷ F. Seitz, *The modern theory of solids*, McGraw-Hill, New York (1940).
- ³⁸ C. Herring and M. H. Nichols, *Rev. Mod. Phys.* **21**, 185 (1949).
- ³⁹ N. D. Lang and W. Kohn, *Phys. Rev. B* **3**, 1215 (1971).
- ⁴⁰ V. Heine and C. H. Hodges, *J. Phys. C* **5**, 225 (1972).
- ⁴¹ N. D. Lang and W. Kohn, *Phys. Rev. B* **8**, 6010 (1973).
- ⁴² J. L. F. Da Silva, C. Stampf and M. Scheffler, *Phys. Rev. Lett.* **90**, 066104 (2003).
- ⁴³ K. M. McCreary, K. Pi, A. G. Swartz, W. Han, W. Bao, C. N. Lau, F. Guinea, M. I. Katsnelson and R. K. Kawakami, *Phys. Rev. B* **81**, 115453 (2010).
- ⁴⁴ M. M. Fogler, D. S. Novikov and B. I. Shklovskii, *Phys. Rev. B* **76**, 233402 (2007).
- ⁴⁵ According to the studies of^{31,36}, Ti is chemically adsorbed in graphene and does not preserve the Dirac point in the newly computed band structure. However, since the maximum concentration of Ti studied by²⁶ is below 1%, one does not expect that in this case the band structure will be significantly changed with respect to pristine graphene.
- ⁴⁶ P. Hohenberg and W. Kohn, *Phys. Rev.* **136**, B864 (1964).
- ⁴⁷ W. Kohn and L. J. Sham, *Phys. Rev.* **140**, A1133 (1965).
- ⁴⁸ The assumption that the cross-capacitance between two clusters S and S' is solely due to the presence of the graphene

plane can be expressed mathematically as $C_{SS'}^{-1} = 2C_{Sg}^{-1} - C_{gg}^{-1}$, where $C_{SS'}^{-1}$, C_{Sg}^{-1} and C_{gg}^{-1} are, respectively, the inverse cross capacitance of two clusters, the inverse cross capacitance between a cluster and the graphene plane and the inverse self-capacitance of graphene. Writing the joint capacitance of two clusters as $\tilde{C}_S^{-1} = C_{SS}^{-1} + C_{S'S'}^{-1} - 2C_{SS'}^{-1} = 2(C_{SS}^{-1} - C_{SS'}^{-1})$, since $C_{S'S'}^{-1} = C_{SS}^{-1}$, and using the equation above, we see that this expression is equivalent to the equality $\tilde{C}_S^{-1} = 2C_S^{-1}$, where $C_S^{-1} = C_{SS}^{-1} + C_{gg}^{-1} - 2C_{Sg}^{-1}$ is the joint capacitance of a cluster and the graphene plane. Note that in the derivation of (4) the assumption that $C_{SSi}^{-1} = C_{Sg}^{-1} + C_{gSi}^{-1} - C_{gg}^{-1}$, i.e. that the cross-capacitance between the clusters and the Si sheet is due to two capacitors in series, is also used.

⁴⁹ O. Madelung, Introduction to solid-state theory, 3rd ed., Springer Verlag, 1996.

⁵⁰ Equation (22) is also valid for a simple capacitor geometry in the absence of deposited metal. In that case, one sees that for the parameters as given in experiments made with capacitor like devices, $|\Omega| \gg \Lambda^2/4$ and hence the doping of graphene is very well described by a simple capacitor law¹, except in the neighbourhood of the Dirac point.

⁵¹ O. K. Andresen, Phys. Rev. B **2**, 883 (1970).

⁵² I. Estermann, S. A. Friedberg and J. E. Goldman, Phys. Rev. **87**, 582 (1952).

⁵³ D. L. Hill and J. A. Wheeler, Phys. Rev. **89**, 1102 (1953).

⁵⁴ J. B. Ketterson and L. R. Windmiller, Phys. Rev. B **2**, 4813 (1970).

⁵⁵ CRC Handbook of Chemistry and Physics, 90th Edition, Taylor and Francis 2009-2010.

⁵⁶ A spherical cluster of Pt atoms with $R = 6$ Å contains approximately 60 atoms of platinum.

⁵⁷ A spherical cluster of Ti atoms with $R = 1.88$ Å contains only 2 atoms of titanium. It is thus debatable if a continuum theory such as the one presented above is applicable. The relative agreement obtained may be accidental, see⁶¹.

⁵⁸ The experimental results of²⁶ allow one to place a limit on the minimal distance between the clusters and the graphene sheet, i.e. $L - R \leq 3$ Å. We have therefore chosen $L - R = 2.5$ Å, although the results for Δ_c are only very weakly dependent on $L - R$, unlike what happens with R .

⁵⁹ The result of references^{35,36} for the induced dipoles was obtained for a system of a single graphene sheet adsorbed on a bulk transition metal and hence does not take into consideration the effect of the finite size of the clusters.

⁶⁰ K.H. Meiwes-Broer, Hyp. Int. **89**, 263 (1994).

⁶¹ The ionisation potential of a Ti cluster computed from (24) is ≈ 7.5 eV. This value is similar to the average ionisation energy of 8.0 eV of an isolated Ti atom, if we consider the average doping of -0.174 e/Ti atom, using the first and second ionisation energies of the titanium atom. The relative coincidence of these two values may help explain why one is still able to apply a continuum theory to describe essentially isolated titanium atoms.

⁶² The computed work-function of graphene adsorbed on (111) platinum in^{35,36} is 4.87 eV with $c_S = 0.75$. This is to be compared with the value of the work function at zero gate voltage obtained from (24) for the largest coverage $c_S = 0.171$ considered above, if we neglect the induced dipole, which is equal to 4.33 eV. Hence, $e\Delta D_g > 0.55$ eV, at large coverages.

⁶³ Performing the spatial averaging of the second term of equation (31) over a disc of radius $\mathcal{R} = \sqrt{\frac{A_g}{\pi}}$, one obtains, to leading order in \mathcal{R} , the result given by equation (29) (multiplied by ϵ_0/e).

⁶⁴ We are grateful to P. Fulde for having called our attention to the need to estimate the ratio ξ , so as to determine the domain of validity of the independent cluster approximation.

⁶⁵ J. Jeans, The mathematical theory of electricity and magnetism, 5th ed., CUP, 1933.

⁶⁶ In order to achieve faster numerical convergence⁶⁵, one should represent $g(\lambda, \xi) = \sum_{n=1}^{s-1} \frac{\lambda^n}{1 - \xi \lambda^{2n}} + \lambda^s \sum_{p=0}^{\infty} \frac{(\xi \lambda^{2s})^p}{1 - \lambda^{2p+1}}$.